Collective migration of an epithelial monolayer in response to a model wound

M. Poujade*, E. Grasland-Mongrain*, A. Hertzog†, J. Jouanneau†, P. Chavrier†, B. Ladoux‡, A. Buguin*, and P. Silberzan*§

*Laboratoire Physico-Chimie Curie (Unité Mixte de Recherche 168), Institut Curie, Centre National de la Recherche Scientifique, Université Pierre et Marie Curie, F-75248 Paris, France; †Laboratoire Compartimentation et Dynamique Cellulaires (Unité Mixte de Recherche 144), Institut Curie, Centre National de la Recherche Scientifique, F-75248 Paris, France; and ‡Laboratoire Matière et Systèmes Complexes (Unité Mixte de Recherche 7057), Université Paris 7, Centre National de la Recherche Scientifique, F-75251 Paris, France

Edited by Robert H. Austin, Princeton University, Princeton, NJ, and approved August 8, 2007 (received for review May 30, 2007)

Using an original microfabrication-based technique, we experimentally study situations in which a virgin surface is presented to a confluent epithelium with no damage made to the cells. Although inspired by wound-healing experiments, the situation is markedly different from classical scratch wounding because it focuses on the influence of the free surface and uncouples it from the other possible contributions such as cell damage and/or permeabilization. Dealing with Madin–Darby canine kidney cells on various surfaces, we found that a sudden release of the available surface is sufficient to trigger collective motility. This migration is independent of the proliferation of the cells that mainly takes place on the fraction of the surface initially covered. We find that this motility is characterized by a duality between collective and individual behaviors. On the one hand, the velocity fields within the monolayer are very long range and involve many cells in a coordinated way. On the other hand, we have identified very active "leader cells" that precede a small cohort and destabilize the border by a fingering instability. The sides of the fingers reveal a pluricellular actin "belt" that may be at the origin of a mechanical signaling between the leader and the followers. Experiments performed with autocrine cells constitutively expressing hepatocyte growth factor (HGF) or in the presence of exogenous HGF show a higher average velocity of the border and no leader.

collective motility | epithelial cells | microfabrication | wound healing

In many physiological situations, the resting cells of an incomplete epithelium become motile under a given stimulation (1). In some cases, the cells dissociate and individually explore their surroundings, whereas in some other instances, they become collectively motile, maintaining cell–cell contacts while invading the free surface. The comparison of these two processes in the framework of the epithelial–mesenchymal transition has strong implications for our understanding of several cancer-related dissemination phenomena (2).

In this article, we focus on the collective motility involved in many different situations, ranging from morphogenesis (3), as illustrated for instance by the dorsal closure in *Drosophila* embryo, to the healing of wounds (4). Interestingly, although very different in nature, these phenomena share many common features (5).

Practically, many aspects of the migratory behavior of cells can conveniently be studied *in vitro* by using the classical "wound-healing" scratch assay, in which a confluent epithelium is scratched with a tool such as a pipette cone or a razor blade, so as to mechanically remove a "strip of cells" from the monolayer. The progression of the remaining cells during the "healing" of this "wound" is then observed under the microscope for durations ranging from a couple of hours to a few days, and the analysis of the cells' progression provides important indications of the motile phenotype of the cells.

Two main mechanisms of healing have been identified (6). The first one, called "purse-string" closure, results from relatively small wounds around which a pluricellular continuous actin belt can develop along the wound border. Healing is then performed by the contraction of this belt via myosin motors (7, 8). The second healing mechanism, more relevant to this article, proceeds by an acquired motility of the border cells, which spread and crawl collectively on the new surface while maintaining the integrity of the epithelium (9). These two mechanisms are actually not exclusive and may coexist in the same wound (10).

In situations where crawling is involved, it is not quite clear what triggers this acquired motility. The scratch process destroys the removed cells, which release their intracellular content into the medium; this process is also quite traumatic for the cells on the newly formed border. Indeed these border cells may become partially permeable as a result of the brutal tearing off of the adhesive junctions they maintain with their neighbors. A sudden influx of the extracellular medium in these cells may potentially trigger their migration. Of course, it is also possible that a free edge is sufficient by itself to generate a motile response. This assumption has been made in a large number of studies but has been verified only in a very limited number of cases dealing with corneal epithelia (11) or endothelial cells (12).

Growth factors and particularly HGF (hepatocyte growth factors) are known to promote scattering and motility of epithelial cells and have a proven effect on healing (13–15). Several theoretical models have thus described the stimulation of the proliferation and migration of the cells by chemical cues such as these growth factors (16–18), including a possible autocrine activity of the border cells (19).

Madin–Darby canine kidney (MDCK) cells are prototypical of epithelial cells that migrate by crawling after a mechanical wound. This migration is associated with small GTPases of the Rho family whose activation is not restricted to the border cells but extends as far as 4–10 cell rows within the epithelium (20). At the same time, as already mentioned, the epithelia keep their integrity; the cell–cell contacts are maintained in particular by cadherins (21), although it has been observed that MDCK cells migrate actively within the monolayer by developing active "cryptic" lamellipodia under the other cells (20). Interestingly, although the onset of migration significantly depends on the initial cell density (22), cell division

Author contributions: B.L., A.B., and P.S. designed research; M.P., E.G.-M., A.H., B.L., A.B., and P.S. performed research; M.P., J.J., P.C., B.L., A.B., and P.S. contributed new reagents/analytic tools; M.P., E.G.-M., A.H., and P.S. analyzed data; and P.S. wrote the paper.

The authors declare no conflict of interest.

This article is a PNAS Direct Submission.

Abbreviations: HGF, hepatocyte growth factor; MDCK cell, Madin–Darby canine kidney cell; PDMS, polydimethylsiloxane; PIV, particle image velocimetry.

See Commentary on page 15970.

§To whom correspondence should be addressed at: Institut Curie, Centre de Recherche, 26 Rue d'Ulm, 75248 Paris Cedex 05, France. E-mail: pascal.silberzan@curie.fr.

This article contains supporting information online at www.pnas.org/cgi/content/full/0705062104/DC1.

does not play an active role but rather appears to redensify the monolayer (20).

Moreover, marginal protrusion activity can be observed along the borders (9). These protrusions can take the appearance of "leader" cells for other epithelial cell types such as IAR2 rat liver cells (23). These leaders are very active and lose some of their epithelial characteristics in particular by developing a Rho-dependent active lamellipodium. They drag some cells behind them as they progress on the surface. However, in these observations, like in many others, it remains unclear whether the observed behaviors are the result of the injury of some cells during scratching or whether they are intrinsic to the acquired motility.

On a more technical side, several techniques for removing cells along a specified geometry in a confluent monolayer have been proposed as an alternative to overcome the intrinsic limitations of scratch-wounding. An interesting improvement is to use laser photoablation (8), which creates well defined, small wounds but still results in possible contributions from destroyed or injured cells next to the new border. Moving further away from the classical approach, the electrical wound assay kills the cells of the epithelium sitting on top of an electrode by applying a voltage pulse (24). However, many cells are destroyed by this procedure (even more than those destroyed by scratching), and many cell fragments remain on top of the electrodes. Furthermore, the damage done to the border cells is unknown. In other studies, an agar block (11), a silicone elastomer sheet (25), or other types of barriers (12) have been used to mask the surface to the cells during the growth of the epithelium. Removing the barrier then presents a free surface to the cells and avoids physical damage. However, conclusions drawn from these studies are still controversial.

In this article, we have combined the strategy of masking with microfabrication to (*i*) precisely define the initial geometrical conditions on a scale of micrometers and (*ii*) make many wounds in parallel so that the performed measurements are supported by good statistics.

We use this original technique to address several key points mentioned above. First, we study the response of a MDCK monolayer to a surface release and identify the parameters that trigger the motility. We then characterize this acquired collective motility by analyzing collective and individual cell behaviors. We end by testing the influence of HGF on these processes.

Results and Discussion

Wounding. First we describe the technique that we have used to present some free surface to the epithelia. Before describing the details of the experiments, we must insist on a point of vocabulary. We call our experiments "wound healing" even though they include no "wound" (no injury) *per se*. Although this expression is somewhat misleading in the present injury-free situation, we use it as a generic term, setting the framework of our work.

Inspired by earlier works (26–28), we used a microfabricated soft elastic "microstencil" consisting of an openwork thin film of crosslinked polydimethylsiloxane (PDMS); the fabrication of the film is described in *Materials and Methods*. The size and shape of the holes, their spacing, and other geometrical parameters are easy to vary by stencil microfabrication. In this article, we discuss only long rectangular openings. The stencils are deposited on the surfaces before plating of the cells, which are then cultured until they reach confluence in the apertures, at which point we remove the stencil, thereby releasing new areas for the cells to migrate to (Fig. 1).

We then observed very well defined linear borders over lengths of the order of a few millimeters (Fig. 2*a*). The mortality of the cells caused by the peeling of the mask was evaluated by using Trypan blue. Less than 5% of the border cells tested positive (none tested positive within the epithelium). Thus we clearly attained the model situation in which free space is offered to the monolayer with minimal damage being made to the cells.

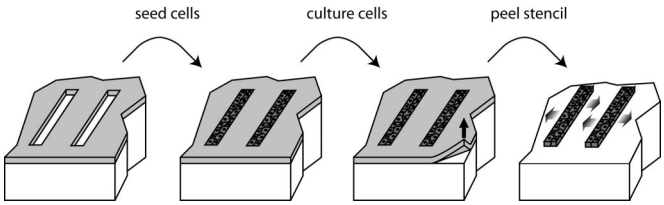

Fig. 1. Principle of the experiments. The cells are cultured on an openware PDMS thin elastic film. When they reach confluence, this microstencil is removed to allow them to collectively migrate.

Migration Triggered by a Model Wound and Advantages of the Assay. Within a couple of hours after the removal of the stencil, the cells became progressively motile in the direction perpendicular to the free edge. Free surface offered to an epithelium is thus sufficient to trigger cell migration (at least with the MDCK cell type).

These observations are compatible with those dealing with corneal epithelia (11) or endothelial cells (12) in the sense that a true injury of the border cells is not necessary to trigger the migration of these cells. This conclusion validates the underlying assumption of many studies dealing with *in vitro* wound healing.

In addition to the lack of injury of the border cells of the monolayer, this microfabrication-based strategy presents several advantages compared with the usual scratch tests. Practically, we have found that scratching monolayers is something of an art. The quality or the aspect of the wound depends on several parameters such as the size or shape of the tool or its velocity when scratching the monolayer as it affects the damage made to the cells (29). Moreover, it is often observed that, after a scratch, the monolayer retracts on both sides of the wound, meaning that, at least transiently, the interactions of many cells with the surface have been disrupted, an effect that also depends on the velocity of scratching (29). We have not observed such an effect with the microstencils based assay. In contrast, we obtain regular, well defined wounds of perfectly controlled width with no particular precaution. The initial conditions are very well defined with a rectilinear edge over distances up to centimeters, giving an absolute origin for the measurement of its progression. Furthermore, as the experiments proceed by removing a mask, there is no debris for the cells to deal with.

We also add a new parameter to these migration studies: the possibility of tuning the chemical composition of the surface to be invaded. In classical wounds, this surface was conditioned by the extracellular matrix that the cells developed during the growth of the monolayer. In our experiment, because there were no cells on the surface before the wound, we could control its chemistry by adequate surface treatments.

We now describe the mean dynamic behavior of the free border of the monolayer and then focus on the details of its structure during healing.

Average Dynamical Behavior of the Border. Like other studies of classical wounds on epithelial monolayers (22, 24), our study showed a nonlinear progression of the free edge. The acquired average velocity accelerated from 0 to 10 ± 5 μm·h^{-1} in typically 15 h. In ref. 22, the dynamic behavior of the mean progression $\langle s \rangle$ of the edge was empirically fitted by a parabolic law. Fitting our data with a power law $\langle s \rangle = a \cdot t^n$ gave results compatible with this parabolic evolution because the average progression for various initial widths was well described by a common exponent $n = 1.8 \pm 0.4$ (Fig. 3, solid symbols) after a few hours. The exact interpretation of this acceleration is still unclear. As the data seem to level off long term, we can't rule out that we actually observed a slow transition toward a constant velocity regime ($n = 1$) after a latency time. Further experiments with more space available to the cells should clarify this point.

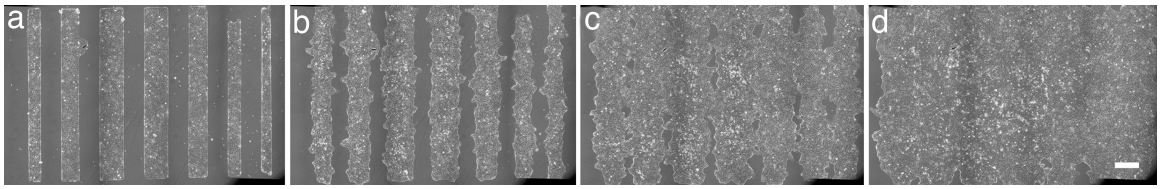

Fig. 2. Sequence of micrographs showing the progression of several bands of different initial widths (*a*, $t = 90$ min; *b*, $t = 13$ h; *c*, $t = 25$ h; *d*, $t = 37$ h). The time $t = 0$ is taken at the removal of the stencil. Each image results from 18 acquisition fields stitched together. (Scale bar: 400 μm.)

The migration of the cells was independent of the width of the initial strip as long as it was larger than 150 μm. Interestingly, when this initial strip was 100 μm ($\approx$8 cell diameters), the progression was slowed down and followed a different dynamics (Fig. 3, open symbols) as the measured exponent n was significantly smaller in that case ($n \sim 1.3$). We interpret this result as a consequence of the small distance between the borders that did not allow them to behave independently and thus slowed down their progression.

Eventually, of course, two opposite borders progressing one toward the other rejoined and closed the wound.

However, such an average description is not sufficient to fully describe the ongoing processes because, at the same time, the roughening of the borders becomes very important. The following discussion goes beyond this description.

Flows Within the Epithelium. To fully characterize the displacements within the epithelium, we have used particle image velocimetry (PIV), a whole-field technique routinely used in hydrodynamics, that consists of extracting the local displacement vectors from the cross-correlation of successive images (30). Thanks to the textures of the phase contrast images, no markers such as beads were necessary.

We found very complex displacement fields that exhibited remarkable long-range correlations (Fig. 4). Although the full analysis of the coherence of the velocity fields is quite complex, requiring the use of biorthogonal decompositions in space and time (31), qualitatively a correlation length could be estimated by using a 2D Fourier transform of the spatial distribution of the velocities, to be on the order of 100 μm. These flows were not necessarily directed toward the free surface as it is illustrated in Fig. 4 (where vertices are observed).

The active implication of the cells several rows behind the border has been identified in the MDCK system (9, 20). Indeed, these references report cells that move actively within the epithelium, in a fibroblast way, by using a so-called "cryptic" lamellipodium that finds its way under the other cells of the monolayer. We demonstrate here that these motions, which propagate well within the monolayer, are not independent but are, on the contrary, highly correlated.

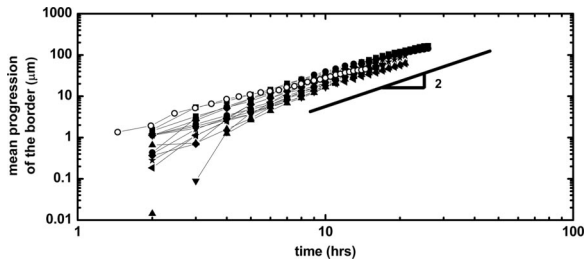

Fig. 3. Dynamic progression of the border of the epithelium. Several experiments performed in similar conditions are reported on the same graph. For the solid symbols, initial widths range from 150 μm to 400 μm. The open symbols represent an experiment with an initial width of 100 μm. The lines are guides for the eye.

Proliferation. The proliferation of the cells has been a concern during our experiments. To test its relevance, we have monitored the number and orientation of the cell divisions during the healing process. During the time-course of an experiment, divisions were almost exclusively (with a proportion close to 85%) located on the initial locus of the band of cells (see Fig. 5). As expected, for times shorter than the division time (18 ± 2 h in our case), the number of cells increased linearly with time; their constant rate of proliferation is comparable to the one measured for the normal growth of these cells [supporting information (SI) Fig. 8*a*]. Interestingly, the cells did not divide along any preferential direction (see SI Fig. 9).

This apparent localization of the divisions in the initial band cannot be accounted for only by a longer presence of the cells in this region. The remaining effect ($\approx$50%) can be attributed to a modification of the underlying substrate by the cells during their growth in the holes of the stencil; during this period, the cells produced extracellular matrix that may be later favorable to the divisions. A second possibility is that the cells that migrated divided less often than those closer to the center, whose proliferation would then compensate for the loss of material due to this migration.

In any case, there is no increase of proliferation in these healing experiments. Experiments performed in the presence of mitomycin C to inhibit proliferation showed similar results (comparable progression and fingering of the edge) for times shorter than $\approx$10 h (data not shown). These observations are in agreement with previous results on similar systems (13, 20). As the monolayer expands at a faster rate than the increase in the number of cells, the cell density is not constant. It first increases before eventually decreasing over time (see SI Fig. 8*b*).

This conclusion is also supported by the lack of preferential orientation of these divisions. Indeed, previous studies have shown that intracellular forces exerted by the actin cytoskeleton control the orientation of the spindle (32). Because we did not observe any preferential direction, we conclude that, on average, no force toward the edges is exerted in the central region of the expending monolayer.

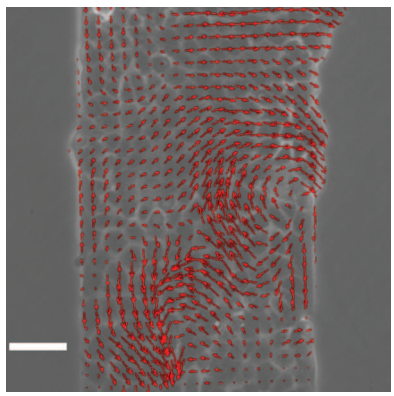

Fig. 4. Snapshot of the velocity field 4 h after removal of the stencil. This image was obtained by PIV (see text for details). The two vertices are an illustration of how coordinated the flows can be but are not a general feature. (Scale bar: 50 μm.)

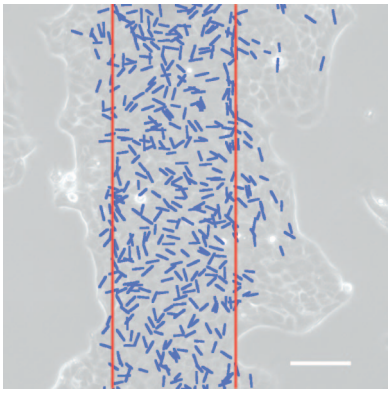

Fig. 5. Cumulative plot of the divisions over a time course of 16 h. Each blue line indicates the position and orientation of the division. The red lines indicate the initial position of the band. A vast majority (85%) of the divisions occur in the locus of this initial band with no particular orientation (see SI Fig. 9). (Scale bar: 100 μm.)

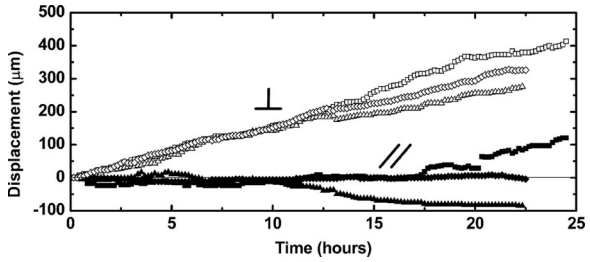

Fig. 7. Progression of the leaders for three independent fingers in two distinct experiments. Time $t = 0$ is taken at the beginning of the finger formation and not at the removal of the stencil. The symbol / / denotes the progression parallel to the initial edge (open symbols), the symbol $\perp$ is used for displacements perpendicular to this initial edge (solid symbols). Leaders thus progress mostly perpendicularly to the initial wound edge at constant velocity.

Roughening of the Border and Leader Cells. It is very clear from the sequence shown in Fig. 2 that, starting from a very linear initial condition imposed by the stencil-based assay, the borders of the wound roughened considerably while they progressed on the surface. However, the quantitative evolution of the contour length revealed that, besides an overall increase in this length after the removal of the stencil, no universal behavior could be observed (data not shown). This diversity in the observed behaviors can be attributed to a fingering destabilization of the border.

Indeed, after typically 1 h, we observed the appearance of leader cells, which were very distinct from the other cells of the border (see Fig. 2*b* and Fig. 6*a*). These leaders were much larger and spread out, and they developed a clear active ruffling lamellipodium and lost their epithelial morphology. In particular, as revealed by fluorescence microscopy, they lost the subcortical actin (Fig. 6*b*) and developed well defined focal adhesions at their leading edge (Fig. 6*c*). However, they maintained cell–cell contacts via cadherins with their "followers," which they dragged to form the fingers (Fig. 6*d*) and which, in contrast, kept their epithelial phenotype. The sides of the fingers also developed a clear pluricellular subcortical actin belt reminiscent of the structures observed in purse-string mechanisms (Fig. 6*b*). These fingers could start at any time during the course of an experiment; their numbers thus increased with time. In some circumstances, we could observe as many as five fingers per millimeter, although their distribution was very heterogeneous.

These leader cells did not systematically originate from the initial border but often arose from the first, second, or third row, thereby excluding the hypothesis of cells damaged at the removal of the mask. When these leader cells were initially within the monolayer, they were brought to the border by the flows mentioned previously, with no observable change in their morphology, their phenotypes then changed drastically, and they lost their epithelial characteristics to become more spread and very motile.

Their dynamic behavior is pictured in Fig. 7. It is markedly different from the average behavior of the border; not only did the cells progress much faster, but they also did it at a constant velocity. For the experiments performed on tissue culture plastic, the velocity v of these fingers was very homogeneous between all of the fingers. We found that $v = 18 \pm 2\ \mu\text{m}\cdot\text{h}^{-1}$ compared with the mean velocity of the border after 10 h; $v_{\text{border}} \approx 10\ \mu\text{m}\cdot\text{h}^{-1}$. These leaders are also characterized by a very high directionality. Once they took a direction, they essentially kept it for the time-course of an experiment and even more so in the first 10 h after their apparition (Fig. 7). For ≈70% of the studied fingers, this direction was normal to the initial border. The leader cells are however transient. As soon as a leader reached the opposite monolayer, it lost its highly motile characteristics to become indiscernible from the other MDCK cells, as it was initially.

We have observed these digitations on several different surfaces (cell-culture plastic, and fibronectin-coated glass or plastic) with comparable aspects, statistics, and velocities. Characteristic focal adhesions such as those observed in Fig. 6*c*, where cells were plated on fibronectin-coated substrates, confirmed however the presence of this extracellular matrix protein. This independence regarding the surface properties may seem surprising at first. However, it has been shown that the effect of fibronectin on cell migration is very dependent on the protein surface concentration (33). As a matter of fact, the effect of fibronectin at the same concentrations as those used in our study has been shown to be very limited on single MDCK cells that became motile under the scattering influence of HGF (33) as well as on the collective migration of endothelial or epithelial cells, regardless of whether a scratch assay (12, 13) or a barrier-based assay (12) was used.

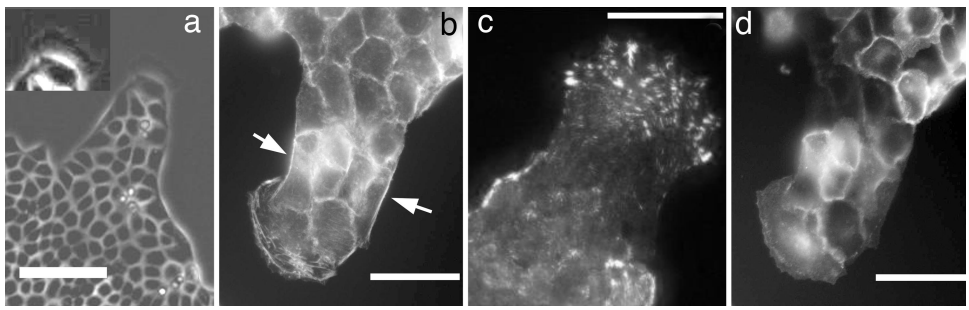

Fig. 6. Micrographs of leader cells 18 h after stencil removal. In each image, a single leader drags a finger. (*a*) Phase contrast image of a finger preceded by a large leader cell. At the leading edge of this leader, there is a very active, ruffling lamellipodium (see *Inset* where the contrast has been enhanced on the same leader). (Scale bar: 100 μm.) (*b*) Fluorescence image of the actin cytoskeleton using Alexa 594-conjugated phalloidin staining. Particularly visible is the subcortical actin belt along the edges of the finger (arrows). (Scale bar: 50 μm.) (*c*) Immunofluorescence total internal reflection fluorescence image of the focal adhesions (vinculin labeling) showing that they are very developed at the leading edge of the leader. (Scale bar: 50 μm.) (*d*) Direct fluorescence image of the E-cadherin–GFP showing the cell–cell adhesions in particular between the leader and the followers. (Scale bar: 50 μm.)

Leader cells have been described in other wound-healing experiments. For instance, ref. 9 describes a "protrusive cell activity" for MDCK cells that looks very similar to the first stage of the fingers drawn by the leaders. For IAR2 rat liver epithelial cells (23), Rho-dependent leader cells were observed and identified as such, although the extension of the fingers was not as large as that described in our study. We believe that we observed much longer fingers because of the injury-free experimental assay used. By avoiding damage to the cells present on the border, the actin belt that might be a critical element by transmitting the mechanical tension is preserved.

In different situations, Haga *et al.* (34) have observed that, on a soft collagen substrate, growing MDCK cell islands migrate collectively, driven by a fibroblast-like leader cell. It is striking to observe similar phenotypes in situations that are so different. Taking a larger perspective, the link between these two sets of experiments might very well be the mechanical triggering of the phenotype (the softness of the substrate or the removal of a physical barrier).

Growth Factors: Communication Between Cells. Leaders are however not restricted to mechanically induced situations. Recent *in vivo* experiments dealing with the development of the lateral line of the zebrafish (35) have also elegantly demonstrated that the development of this line proceeds by the isolation of a leader driving the other cells in response to an external chemotactic cue.

HGF has been proven to strongly accelerate healing in some circumstances, although for high concentrations, its scattering effect can actually be detrimental (13). Thus we have performed experiments by adding low-concentration HGF to the medium or by using autocrine cells constitutively producing HGF. In both cases, the HGF concentration (≈10 ng/ml) was too low to induce scattering, but healing was indeed accelerated by ≈50%, which is consistent with the reported effect of HGF at this concentration (13). However, no leader or, *a fortiori*, finger was observed, although the border cells did develop limited lamellipodia (see SI Fig. 10).

HGF thus suppressed the fingering of the border. Whether it transformed all of the border cells into leaders, as the presence of lamellipodia may indicate, or it activated a different mechanism is however still debatable. In the presence of HGF, cell–cell contacts appeared much weaker with, in some cases, cells transiently dissociating from the epithelium. We correlate this last observation with the internalization of the cadherins (36), a well known effect of HGF that was not observed in the healing experiments performed in the absence of HGF (Fig. 6*d*). Besides, in the case of IAR-2 epithelial cells, leaders are more abundant in the case of dominant negative RhoA cells, and this phenotype disappears with constitutively active RhoA (23). Among other effects, HGF tends to activate Rho, leading to the formation of stress fibers (37). We therefore tend to believe that the effects of wounding and HGF are different.

Conclusion

We conducted an original injury-free wound-healing assay on MDCK epithelial cells. Under these conditions, we have demonstrated that free surface is sufficient to trigger cell migration. We observed both extremely complex and coordinated long-range motions within the epithelium, and a fingering of the borders preceded by transient leader cells that have a very nonepithelial, fibroblast-like appearance and behavior. The high concentration of actin in a pluricellular subcortical actin belt along the fingers may be indicative of a strong mechanical tension and signaling between the leader and its followers. These observations support the hypothesis of a mechanical means of communication between the cells in response to the free surface.

Technically, the stencil-based assay is an advantageous alternative to classical scratch tests. In addition to the advantages outlined in the text, this assay offers a solution for parallel testing, which is notoriously difficult when using robots that scratch simultaneously many monolayers in multiwells plates (38).

This ability to make many wounds in parallel in a single step can also be used to efficiently analyze the proteic content in the supernatant or in the cells after extraction. Indeed, making many wounds and thus many borders at the same time is often performed to this end by scratching the epithelium in many locations or by using more sophisticated devices that are specially designed to achieve this result (39). With the stencil-based method presented here, scales typically go down to a few 100 μm. Compared with the standard technique, this strategy allows us to make at least 10 times as many perfectly identical wounds, and thus to gain an order of magnitude in concentrations and potentially in sensitivity, while retaining the advantages outlined above. Furthermore, this technique enables us to quantify the total length of the borders and thus to quantitatively correlate the detected species with this parameter.

Last, we reflect on the tubulogenesis of these epithelial kidney cells whose molecular aspects have been extensively studied (40). If epithelia are capable of forming fingers on a plane surface such as those used in the experiments presented in this article or spontaneously follow a leader on soft surfaces (34), it seems natural to ask whether this mechanical signaling can also be part of morphogenetic processes in the formation of complex tridimensional structures.

Materials and Methods

Microfabrication of the Stencils. Microstencils were molded in PDMS elastomer (Sylgard 184, Dow Corning) on a photoresist template according to a procedure inspired by the one described in ref. 26.

Briefly, 30- to 100-μm-thick rectangular prism structures were fabricated in negative photoresist (SU8-2025 or SU8-2075, Microchem) by conventional photolithography. Uncured PDMS was then poured on this template and pressed against it in a homemade four-screw press so that the resist structures came through the elastomer. This whole set-up was cured at 65°C for 12 h and assembled in a second step with a thick PDMS frame to allow easier subsequent handling. The cross-linked PDMS film was then slowly peeled off and washed in detergent (Nalgene L900) for several hours, rinsed, air-dried, and UV sterilized directly before use. By using the same procedure, we were able to reuse the same stencils several times without any noticeable change in the observed results.

Cell Culture. Several MDCK cell lines were used. The wild-type MDCK cell line and the HGF-autocrine cell line derived from it are described in ref. 41. In some experiments, we also used a stable clone of MDCK cells expressing E-cadherin–GFP with no difference in our experiments compared with wild-type cells.

The cells were cultured in Dulbecco's modified Eagle's medium (Gibco) supplemented with 10% FBS (Sigma), 2 mM L-glutamin solution (Gibco), and 1% antibiotics solution [penicillin (10,000 units/ml) + streptomycin (10 mg/ml); Gibco] at 37°C, 5% CO_2, and 90% humidity.

When indicated, HGF (Sigma) was added at a concentration of 10 ng/ml 2 h before the removal of the stencil.

Mitomycin (Sigma) was added when the stencil was removed to a final concentration of 5 μg/ml, effectively inhibiting proliferation. Signs of toxicity were observed after 12 h. Therefore, only times shorter than 10 h were analyzed.

Model Wounds. Bare or fibronectin-coated, sterile, culture-treated plastic 35-mm Petri dishes and six-well plates were used for the video-microscopy experiments. Fibronectin-coated glass slides were used for all of the immunofluorescence experiments. The fibronectin-coating process was performed by incubating the sur-

face for at least 1 h at 37°C in a 10 μg/ml solution of fibronectin (Sigma) in PBS.

Microstencils were then deposited on the chosen surface, and cells were cultured for typically 12–24 h in the incubator (37°C, 5% CO_2, 90% relative humidity). Longer incubation times were avoided because they tend to promote some adhesion of the cells on the PDMS.

After this step, the microstencils were gently peeled off with forceps. The exact cell densities (4×10^5 to 6×10^5 cells/cm^2) were measured *a posteriori* on the images.

To evaluate the viability of the cells after removal of the stencil, cells were rinsed with PBS and then incubated for 5 min with 1.25 ml of a 0.07% solution of Trypan blue (Gibco), after which the number of colored cells was manually counted over a population of ≈1,500 cells representing a total border length of 2 cm.

Fluorescence Microscopy. Cells grown to confluence on glass coverslips coated with fibronectin (Sigma; 10 μg/ml) were observed 18 h after the stencil was removed. They were first fixed in 4% paraformaldehyde (Sigma) in PBS, permeabilized with 0.1% Triton X-100, and blocked with 2% BSA (Sigma). E-cadherin and actin were observed on the same E-cadherin–GFP-expressing cells and vinculin with the wild type. Vinculin labeling was performed by incubation with a mouse monoclonal anti-vinculin antibody (Sigma; 1:400) before staining with Alexa 594-conjugated goat anti-mouse antibody (Molecular Probes, 1:500). For actin, we used Alexa 594-conjugated phalloidin (Molecular Probes; 1:400). The cells were finally mounted with DakoCytomation Fluorescent Mounting Medium (Dako). Images were acquired in epifluorescence for cadherins and actin on a fluorescence microscope (Leica CTR6000). For vinculin, we used a commercial total internal reflection fluorescence attachment (Olympus) on the microscope (Olympus IX-71).

Time-Lapse Microscopy. Time-lapse multifield experiments were performed in phase contrast on an automated inverted microscope (Leica DM-IRBE) equipped with thermal and CO_2 regulations. High-resolution, large-field-of-view images were routinely obtained by stitching together typically 20 fields acquired with 10× or 20× objectives. The size of one pixel could then be as small as 1.25 μm for a field of view of several millimeters. The displacements of the sample and the acquisitions with a CCD camera (EZ CoolSnap, Roper) were controlled through Metamorph (Universal Imaging) software. The typical delay between two successive images of the same field was set to 5 min.

Image Processing. Most of the image processing was performed using the ImageJ public domain software (42). Larger fields were reconstructed from several slightly overlapping fields by using a homemade macro. The average position $\langle s \rangle$ of the border on a given length L could then be calculated according to the following formula: $\langle s \rangle = \frac{1}{L} \cdot \int_0^L y(x)\,dx$, where $y(x)$ is the position of the border at the abscissa x. In our experiments, L was typically 1 mm.

The motions of the leader cells were followed by tracking them manually or by building local kymographs.

The time evolution of the cell population and the orientation of the divisions in a cell stripe were mapped manually.

PIV. The velocity field in the monolayer was mapped by PIV analysis (30, 43). Stacks of images were analyzed by using the MatPIV software package (44) for MatLab (MathWorks Inc.).

The time between successive analyzed images was 15 min. The window size was set to 32 or 64 pixels with no noticeable difference.

We thank R. Austin, M. Bornens, J. Camonis, J.-F. Joanny, and A. Nicolas for fruitful discussions and support, and S. Shvarstman for providing us a preprint of ref. 25. We thank the members of the Unité Mixte de Recherche 144 for providing us the various antibodies, the staff of the imaging platform of the Curie research center, and in particular J.-B. Sibarita for his help in the first experiments. Finally, we gratefully acknowledge funding from the Ligue Nationale Contre le Cancer, the Fondation de France, and the Association pour la Recherche sur le Cancer.

1. Friedl P (2004) *Curr Opin Cell Biol* 16:14–23.
2. Thiery J-P, Sleeman J (2006) *Nat Rev Mol Cell Biol* 7:131–142.
3. Wood W, Jacinto A, Grose R, Gale J, Wilson C, Martin P (2002) *Nat Cell Biol* 4:907–912.
4. Nobes CD, Hall A (1999) *J Cell Biol* 144:1235–1244.
5. Martin P, Parkhurst S (2004) *Development (Cambridge, UK)* 131:3021–3034.
6. Jacinto A, Martinez-Arias A, Martin P (2001) *Nat Cell Biol* 3:E117–E123.
7. Kiehart DP (1999) *Curr Biol* 9:R602–R605.
8. Tamada M, Perez TD, Nelson WJ, Sheetz MP (2007) *J Cell Biol* 176:27–33.
9. Fenteany G, Janmey PA, Stossel TP (2000) *Curr Biol* 10:831–838.
10. Bement WM, Forscher P, Mooseker MSA (1993) *J Cell Biol* 121:565–578.
11. Block ER, Matela AR, SundarRaj N, Iszkula ER, Klarlund JK (2004) *J Biol Chem* 279:24307–24312.
12. van Horssen R, Galjart N, Rens JAP, Eggermont AMM, ten Hagen TLM (2006) *J Cell Biochem* 99:1536–1552.
13. Sponsel HT, Beckon R, Hammind W, Anderson RJ (1994) *Am J Physiol Renal Physiol* 267:257–264.
14. Zhuang S, Dang Y, Schnellmann RG (2004) *Am J Physiol Renal Physiol* 287:F365–F372.
15. Kurten RC, Chowdhury P, Sanders RC, Pittman LM, Sessions LW, Chambers TC, Lyle CS, Schnackenberg BJ, Jones SM (2005) *Am J Physiol Cell Physiol* 288:C109–C121.
16. Sherratt JA, Murray JD (1990) *Proc R Soc London Ser B* 241:29–36.
17. Owen MR, Sherratt JA, Myers SR (1999) *Proc R Soc London Ser B* 266:579–585.
18. Sheardown H, Cheng YL (1996) *Chem Eng Sci* 51:4517–4529.
19. Shvartsman SY, Wiley HS, Deen WM, Lauffenburger DA (2001) *Biophys J* 81:1854–1867.
20. Farooqui R, Fenteany G (2005) *J Cell Sci* 118:51–63.
21. Kametani Y, Takeishi M (2007) *Nat Cell Biol* 9:92–98.
22. Rosen P, Misfeldt DS (1980) *Proc Natl Acad Sci USA* 77:4760–4763.
23. Omelchenko T, Vasiliev JM, Geland IM, Feder HH, Bonder EM (2003) *Proc Natl Acad Sci USA* 100:10788–10793.
24. Keese CR, Wegener J, Walker SR, Giaever I (2004) *Proc Natl Acad Sci USA* 101:1554–1559.
25. Nikolić DL, Boettiger AN, Bar-Sagi D, Carbeck JD, Shvartsman SY (2006) *Am J Physiol Cell Physiol* 291:68–75.
26. Tourovskaia A, Barber T, Wickes BT, Hirdes D, Grin B, Castner DG, Healy KE, Folch A (2003) *Langmuir* 19:4754–4764.
27. Ostuni E, Kane R, Chen CS, Ingber D, Whitesides GM (2000) *Langmuir* 16:7811–7819.
28. Folch A, Jo B-H, Hurtado O, Beebe D, Toner M (2000) *J Biomed Mater Res* 52:346–353.
29. Thiekele H, Impidjati, Fuhr GR (2006) *J Phys Condens Matter* 18:S627–S637.
30. Raffel M, Willert C, Kompenhans J (1998) *Particle Image Velocimetry: A Practical Guide* (Springer, Berlin)
31. Aubry N, Guyonnet R, Lima R (1991) *J Stat Phys* 64:683–739.
32. Théry M, Racine V, Pépin A, Piel M, Chen Y, Sibarita J-B, Bornens M (2005) *Nat Cell Biol* 7:947–953.
33. de Rooij J, Kerstens A, Danuser G, Schwartz MA, Waterman-Storer CM (2005) *J Cell Biol* 171:153–164.
34. Haga H, Irahara C, Kobayashi R, Nakagaki T, Kawabata K (2006) *Biophys J* 88:2250–2256.
35. Lecauday V, Gilmour D (2006) *Curr Opin Cell Biol* 18:1–6.
36. Fujita Y, Krause G, Scheffner M, Zechner D, Leddy HE, Behrens J, Sommer T, Birchmeier W (2002) *Nat Cell Biol* 4:222–231.
37. Royal I, Lamarche-Vane N, Lamorte L, Kaibuchi K, Park M (2000) *Mol Biol Cell* 11:1709–1725.
38. Yarrow JC, Perlman ZE, Westwood NJ, Mitchison TJ (2004) *BMC Biotechnol* 4:21.
39. Turchi L, Chassot AA, Rezzonico R, Yeow K, Loubat A, Ferrua B, Lenegrate G, Ortonne J-P, Ponzio G (2002) *J Invest Dermatol* 119:56–63.
40. Hogan BLM, Kolodziej PA (2002) *Nat Rev Gen* 3:513–523.
41. Bellusci S, Moens G, Thiery JP, Jouanneau J (1994) *J Cell Sci* 107:1277–1287.
42. Rasband WS (2007) ImageJ (National Institutes of Health, Bethesda). Available at http://rsb.info.nih.gov/ij/.
43. Adrian RJ (2005) *Exp Fluids* 39:159–169.
44. Sveen JK (2005) MatPIV (Univ of Oslo, Oslo). Available at http://www.math.uio.no/~jks/matpiv/.